

A Study of Charge Radii and Neutron Skin Thickness near Nuclear Drip Lines

VIRENDER THAKUR[†], SHASHI K DHIMAN[‡]

Department of Physics, Himachal Pradesh University, Summer-Hill,
Shimla-171005, INDIA

We studied the charge radius, rms radius and neutron skin thickness Δr_{np} in even-even isotopes of Si, S, Ar and Ca and isotones of $N = 20, 28, 50$ and 82 . The Δr_{np} in doubly-magic ^{48}Ca , ^{68}Ni , $^{120,132}\text{Sn}$ and ^{208}Pb nuclei has also been calculated. Theoretical calculations are done with the Hartree-Fock-Bogoliubov theory with the effective Skyrme interactions. Calculated theoretical estimates are in good agreement with the recently available experimental data. The charge radii for Si, S, Ar and Ca isotopes is observed to be minimum at neutron number $N = 14$. The theoretically computed results with UNEDF0 model parameterization of functional are reasonably reproducing the experimental data for Δr_{np} in ^{48}Ca , ^{68}Ni and $^{120,132}\text{Sn}$. The energy density functional of UNEDF1 model provides much improved result of Δr_{np} for ^{208}Pb .

Keywords: Hartree-Fock-Bogoliubov; Skyrme Energy Density Functional; Nuclear many-body theory; Charge distributions; Self-consistent mean field

PACS numbers: 21.60.Jz; 21.10.Ft; 21.10.Gv

1. Introduction

Appreciable experimental progress in producing and analyzing exotic nuclei [1, 2] has brought renaissance of nuclear structure models. In recent years [3, 4, 5, 6], The production of more and more new isotopes has revived the interest in nuclear structure models. In nuclear physics, understanding the structure of the atomic nucleus is one of the key challenges. The study of those nuclei which are lying far from the line of β -stability play a crucial role in the understanding of nuclear physics. The limit of nuclear existence is reached while going far away from stability line. An unbound nuclear system disintegrates quasi- instantaneously (in a time interval of the order

[†] virenthakur123@gmail.com

[‡] shashi.dhiman@gmail.com

of 10^{-21} s. Points on the nuclear chart which corresponds to nuclei that are unbound to proton or neutron emissions in the ground state is called the proton or neutron drip line. These drip lines form the edges of the nuclear chart. About 280 stable nuclear species are found on Earth but, according to latest estimates, from 5000 to 7000 bound nuclei should exist in the Universe. Till today, about 2000 in numbers have been synthesized and observed. Very little information is available about these unstable nuclei. Even though the number of undiscovered bound nuclei is very large but we are able to make single big steps by studying a few of specific nuclei. These nuclei act as milestones in setting new effects that arise in extreme conditions of isospin asymmetry. We have chosen Si, S, Ca and Ar nuclei for our interest as lot of research has been done on these nuclei recently [7, 8, 9, 10, 11, 12]. The microscopic structure of these nuclei is of particular interest for the field of astrophysics: the neutron-rich $N \simeq 28$ nuclei play an important role in the nucleosynthesis of the heavy Ca-Ti-Cr isotopes [13]. As these nuclides also become experimentally accessible [13, 14], they can provide a testing ground for studying exotic nuclei.

Exotic nuclei, particularly those near the drip lines, are at the core of one of the fundamental questions driving nuclear structure and astrophysics today: What are the limits of nuclear binding? These Exotic nuclei play a critical role in both informing theoretical models as well as in our understanding of the origin of the heavy elements. Of the nuclei considered here, those with $N = Z$ (^{28}Si , ^{32}S , ^{36}Ar and ^{40}Ca) have been studied extensively both theoretically and experimentally. Among different theoretical approaches used are the shell-correction approach [15], Hartree-Fock [16, 17] and Hartree-Fock-Bogolyubov methods [18], relativistic mean field [19, 20, 21, 22], shell model [23, 24], α -cluster model [24] and others.

To throw some light on the physics of exotic neutron-rich and magic-nuclei near drip lines, we performed calculations based on the self-consistent mean-field theories: Hartree-Fock-Bogoliubov (HFB) with the Skyrme effective interactions approach. The physical observables of interest are nuclear root mean square radius (R_{rms}), nuclear charge radius (R_c) and neutron skin thickness (Δr_{np}). The nuclear charge radius is one of the most fundamental nuclear properties that describes the effect of effective interactions on nuclear structure [43, 25]. It can be measured experimentally by methods based on the electromagnetic interaction between the nucleus and electrons or muons. One of the parameter that can be expressed through the nucleon density distribution is neutron skin thickness which depends on the properties of the nuclear surface. For large neutron excess, the bulk of neutron density is believed to extend beyond the proton density creating a sort of "neutron skin". To determine the nature of the neutron distribution accurately in a nuclei has received considerable attention in recent years

[28, 26, 27]. As neutron number increases, the radius of the neutron density distribution becomes larger than that of the protons, reflecting the pressure of the symmetry energy.

2. Theoretical Framework

The present study has been done by using the model based on Hartree-Fock-Bogoliubov Theory [32, 33]. A brief discussion of the theory is given below.

In this theory, the pairing field and the mean field are given equal footings. Zero range Skyrme interactions are used in the self consistent mean field part [34]. For the Skyrme forces, The HFB Energy has the form of local energy density functional [30, 37]:

$$E[\rho, \tilde{\rho}] = \int d^3r \mathcal{H}(r) \quad (1)$$

where

$$\mathcal{H}(r) = H(r) + \tilde{H}(r) \quad (2)$$

is the sum of the mean-field and paring energy densities. The wave function Φ depends upon the density matrix ρ and the pairing tensor κ and in terms of these two parameters, the HFB energy takes the form [30]:

$$E[\rho, \kappa] = \frac{\langle \Phi | H | \Phi \rangle}{\langle \Phi | \Phi \rangle} = Tr \left[\left(e + \frac{1}{2} \Gamma \right) \rho \right] - \frac{1}{2} Tr [\Delta \kappa^*] \quad (3)$$

where Γ is Hartree-Fock potential and Δ stands for the pairing potential. They are defined in their explicit form as

$$\Gamma_{n_1 n_3} = \sum_{n_2 n_4} \bar{v}_{n_1 n_2 n_3 n_4} \rho_{n_4 n_2}, \quad \Delta_{n_1 n_2} = \frac{1}{2} \sum_{n_3 n_4} \bar{v}_{n_1 n_2 n_3 n_4} \kappa_{n_3 n_4} \quad (4)$$

This leads to the HFB Hamiltonian matrix [30]:

$$\begin{pmatrix} h^{(q_k)} - \lambda^{(q_k)} & \tilde{h}^{(q_k)} \\ \tilde{h}^{(q_k)} & -h^{(q_k)} + \lambda^{(q_k)} \end{pmatrix} \begin{pmatrix} U_k \\ V_k \end{pmatrix} = E_k \begin{pmatrix} U_k \\ V_k \end{pmatrix} \quad (5)$$

where E_k denotes the quasiparticle energies, and λ^{q_k} represent chemical potential. The matrices

$$h_{\alpha\beta}^{(q)} = \langle \Phi_\alpha | h_q | \Phi_\beta \rangle, \quad \tilde{h}_{\alpha\beta}^{(q)} = \langle \Phi_\alpha | \tilde{h}_q | \Phi_\beta \rangle \quad (6)$$

are defined for a given proton ($q_k = +1/2$) or neutron ($q_k = -1/2$) block [30].

3. Results And Discussions

We present our results for root mean square radii and charge radii reflecting size of the nucleus. Neutron skin thickness for isotopes of Si, S, Ar and Ca with particular reference to the disappearance of magic number $N = 28$ with $Z = 14$ in ^{42}Si [39] nuclei has also been analysed. Beside this, the shell structure evolution, nuclear radii and neutron skin thickness in the isotones at $N = 20, 28, 50$ and 82 and doubly magic nuclei in ^{48}Ca , $^{68,78}\text{Ni}$, $^{120,132}\text{Sn}$ and ^{208}Pb have also been investigated. The theoretical results are computed from Axially deformed solution of the Skyrme-Hartree-Fock-Bogoliubov equations using the harmonic oscillator basis [30, 37], where the mean field potentials are constructed with UNEDF0 and UNEDF1 parameterizations [31, 29].

3.1. Size of the Nucleus

Nuclear radii of proton and neutron distributions are the key observables to determine the size of the nuclear system. Even, these observables can be directly related to fundamental bulk properties of nuclear matter and also to the nature of nuclear interactions [41, 42]. In exotic neutron-rich and heavy nuclei the excess of neutrons give rise to a neutron skin to the size of a nuclear system such as; nuclear charge radii, neutron distributions and neutron skin thickness have been found to correlate empirically with a number of observables in finite nuclei [43] to neutron matter [41, 42, 44]. Hence, it further beautifully links with a plausible constraints found to impose on the equations of state high density matter in neutron stars [45].

The goal of this section is to understand the relations between nuclear charge and neutron radii, and compare our theoretical results with available experimental data.

Here in Fig. (1), results for the root mean square radius R_{rms} in fm plotted as a function of nuclear neutron number N , for the even-even exotic to stable nuclides of Si (green left triangles), Sulphur (blue right triangles) Ar (maroon circles) and Ca (red squares). It can be seen from Fig. (1) that the RMS radii of the proton-rich or neutron-rich lie away from the solid line of radii of stable nuclear systems. In case of proton rich nuclei, the values of RMS radii are smaller due to the smaller neutron distributions as compared to neutron rich nuclei. That is why, the theoretically calculated points showing RMS radius for exotic even-even nuclei of Si, S, Ar and Ca for proton rich nuclei as shown in Fig. (1) lies little above from the stability curve. But, for the neutron rich nuclei the theoretically calculated points for the RMS radius of all the four nuclei (Si, S, Ar and Ca) lies little lower than the stability curve. The solid line here represents the stability curve

for the given mass region of nuclides which is computed by using formula $R = R_0 N^{1/3}$.

The results for the charge radii R_{ch} in fermi meter as a function of nuclear mass number A for the nuclides of Argon, Calcium, Silicon and Sulphur are shown in Figs. (2 and 3). The theoretical charge radius is calculated using the formulae [46] :

$$R_{ch} = \sqrt{r_p^2 + 0.64} \text{ fm} \quad (7)$$

where, r_p denotes the rms radius of the proton density distribution and term 0.64 fm^2 accounts for the finite size of proton. The experimental measurements of R_{ch} are also shown for comparison and represented by symbol diamond with error bars [43].

It is clear from Figures that, those nuclei which lie in the proton drip line and the neutron drip line have larger charge radius in comparison to the other stable nuclei. The value of the charge radius is found to be minimum for ^{28}Si nucleus with $N = Z = 14$ as shown in upper panel of Fig. (2), ^{30}S nucleus with $N = 14$ and $Z = 16$ in lower panel of Fig. (2), ^{32}Ar with $N = 14$ and $Z = 18$ in upper panel of Fig., indicating sub-shell closure with $d_{5/2}$ occupying neutron N or proton $Z = 14$, as recently investigated $Z = 14$ sub-shell closure in ^{42}Si nucleus [52]. The theoretical results are producing the experimental data of charge radii R_{ch} in isotopes in Si, S, Ar and Ca with the UNEDF0 parameterizations [31]. Similarly, the variation of charge radii R_{ch} in fm as a function of nuclear mass number for various isotones of $N = 20, 28, 50$ and 82 against Atomic Number (Z) are displayed in Figs. (4 and 5). The experimental results are also shown in Figures for comparison with theoretical values. It can be observed from the Figures that EDF parameterizations (UNEDF0) are reproducing experimental data of charge radii. In case of $N = 20$ isotones, the experimental data is available for nuclides with $A = 36$ to $A = 40$ (^{36}S , ^{38}Ar and ^{40}Ca) as shown in upper panel of Fig. For $N = 28$, the experimental data is available for nuclides with $A = 46$ to $A = 54$ (^{46}Ar , ^{48}Ca , ^{50}Ti , ^{52}Cr and ^{54}Fe) as shown in lower panel of Fig. (5) In case of $N = 50$ isotones, the experimental data taken from ref [43] is available for for the nuclides with mass number $A = 86$ to $A = 92$ (^{86}Kr , ^{88}Sr , ^{90}Zr and ^{92}Mo) as shown in upper panel of Fig. (5) However for $N = 82$, we have experimental results for $A = 132$ to $A = 152$ (^{132}Sn , ^{134}Te , ^{136}Xe , ^{138}Ba , ^{140}Ce , ^{142}Nd , ^{144}Sm , ^{146}Gd , ^{148}Dy , ^{150}Er and ^{152}Yb) as shown in lower panel of Fig. (5), and our theoretical estimates are in good agreement with these experimental results.

3.2. Neutron Skin Thickness

The neutron skin thickness Δr_{np} is defined as the difference between the nuclear rms radii obtained using the density distributions for point neutrons and point protons, i. e.,

$$\Delta r_{np} = \sqrt{r_n^2} - \sqrt{r_p^2}, \quad (8)$$

where r_n refer to the neutron rms radius and r_p denote the proton rms radius. It is well understood from the ref. [44] that the accurate measurement of the neutron skin thickness would place rigid constraints on the density dependence of the nuclear symmetry energy denoted as $S(\rho)$. The density dependence of the nuclear symmetry energy have direct consequences in finite nuclear matter and nuclear dense matter of astrophysical interest. This is why, it is investigated extensively from both theoretical and experimental perspectives. Within available experimental technology in nuclear physics, the nuclear symmetry energy can not be measured directly but the information of this fundamental quantity can be extracted from the neutron skin thickness and electric dipole polarizability [40]. Whereas, the direct measurement of neutron distribution is also extremely difficult, therefore, the recent experimental probes have focused on the accurate measurements of electric dipole polarizability α_D in ^{208}Pb [47], ^{120}Sn [48] and ^{68}Ni [49], while for the extraction of α_D in ^{48}Ca by the Darmstadt-Osaka collaboration is working on at Jefferson Laboratory [50]. These nuclei are very interesting from point of view of nuclear structure physics, because they are neutron-rich and doubly magic nuclear systems, can be understood with recently developed *ab-initio* nuclear density functionals theory. The studies of these nuclear structure observable can provide a constraint for the size of neutrons star [42].

In the Fig. (6), we present the neutron skin thickness $\Delta r_{np} = r_n - r_p$ in fm, plotted as a function of nuclear mass number A , for the chain of even-even exotic isotopes of Silicon (green left triangles), Sulphur (blue right triangles), Argon (maroon circles) and Calcium (red squares). The theoretical estimates are computed from Axially deformed solution of the Skyrme-Hartree-Fock-Bogoliubov equations using the harmonic oscillator basis model (HFB+HO), based on EDF parameterization UNEDF0. The magnitudes of skin thickness is increasing systematically with increase in the neutron number in the isotopes in all the elements.

In case of isotones, whose results are shown in Figs. (7 and 8), we find that there is decrease in the neutron skin depth with increase in atomic number (Z) which signifies that with increase in proton number, there is decline in neutron density. This is because of the fact that as the proton number

raises, the r_p value also increases while the neutron density is unaffected. We have taken in account the isotonic chains of $N = 20$, $N = 28$.

Fig. (7) presents the neutron skin thickness in isotones corresponding to neutron shell closures at magic $N = 20$ (upper panel) and $N = 28$ (lower panel). In upper panel of Fig. (7), we present the neutron skin thickness $\Delta r_{np} = r_n - r_p$ in fm, plotted as a function of atomic number Z , for the even-even isotonic chain of $N = 20$, for ^{28}O , ^{30}Ne , ^{32}Mg , ^{34}Si , ^{36}S , and ^{38}Ar nuclei. It can be seen that the magnitude of the skin thickness is decreasing as on increasing the proton numbers except for ^{34}Si with $Z = 14$, where it rises a little bit from the previous nuclei (^{32}Mg) as calculated from HFB+HO model with Parameterization UNEDF0. Neutron skin thickness varies from 0.10 – 0.7 fm in magnitude. The ^{28}O nucleus has large Δr_{np} magnitudes of about 0.7 fm computed with HFB+HO model due to the larger expected neutron distributions than proton numbers. Whereas, in case of ^{42}Ti nucleus where $Z = 22$ and $N = 20$, the magnitude of the $\Delta r_{np} = 0.10$ fm, is very small.

In lower panel of Fig. (7), we present the neutron skin thickness $\Delta r_{np} = r_n - r_p$ in fm, plotted as a function of atomic number Z , for even-even isotones of neutron shell closure at $N = 28$ for ^{40}Mg , ^{42}Si , ^{44}S , ^{46}Ar , ^{48}Ca , ^{50}Ti and ^{52}Cr . The recent observation of ^{40}Mg [51] provides a significant advancement in our understanding of where the neutron drip line is likely to go for nuclei with atomic number 12. In this isotopic chain we get maximum value of Δr_{np} ranging as 0.65-0.76 fm for ^{40}Mg and ^{42}Si . The discovery of ^{42}Si [52] indicates the strong evidence for a well-developed proton sub-shell closure at $Z = 14$ (14 protons), the near degeneracy of two different ($s_{1/2}$ and $d_{3/2}$) proton orbits in the vicinity of ^{42}Si nucleus. Therefore ^{42}Si nucleus has become the focus of particular interest in discussions of nuclear shell structure at the neutron drip line.

In Fig. (8), we present the theoretically computed results of neutron skin thickness Δr_{np} for the chain of isotones for neutron numbers at magic number 50 (upper panel) and 82 (lower panel). The magnitude of Δr_{np} is being obtained as 0.021 fm in ^{94}Ru and 0.36 fm in ^{78}Ni from HFB+HO model. The theoretical value of Δr_{np} in doubly magic ^{132}Sn nucleus is 0.26 fm, which is comparable with recent experimental extractions of Δr_{np} 0.23 ± 0.02 fm [53] and 0.29 ± 0.04 fm [54]. Lower panel of Fig. (8) presents the variation in Δr_{np} for isotones from atomic number 46 (^{128}Pd) to 68 (^{150}Er) and, the magnitude of skin thickness varies as 0.005 fm in ^{150}Er - 0.32 fm in ^{128}Er and 0.01 fm in ^{150}Er - 0.33 fm in ^{128}Pd , corresponding to HFB+HO parameterization (UNEDF0). The values of Δr_{np} decrease as the atomic number Z is increasing in the chain of isotones shown in Fig. (8) At last, in Fig. (9), we present our theoretical results of neutron skin thickness for neutron-rich doubly-magic nuclei ^{48}Ca , ^{132}Sn , ^{208}Pb and ^{68}Ni , ^{120}Sn the

computed results are compared to the recently available experimental data [48, 47, 49, 55, 56, 57, 58, 62]

extractions [53, 54, 59, 60, 63, 64, 65]. There are many theoretical and experimental investigations focused on ^{208}Pb , ^{132}Sn , ^{120}Sn , ^{68}Ni and ^{48}Ca nuclei, which have well understood nuclear structure due to their closed protons and neutrons shells at the magic numbers. A recent reviews on experimental measurements of Δr_{np} in ^{208}Pb [57], suggest that its values ranges from 0.15 ± 0.03 fm to 0.22 ± 0.04 fm [57], with the analysis of coherent pion photo-production and pion scattering, respectively. Whereas our theoretical results for $\Delta r_{np} = 0.17$ fm in ^{208}Pb are reasonable well within the experimental measurements.

In Fig. (9), we have also presented and compared our results of Δr_{np} for ^{132}Sn , ^{120}Sn , ^{68}Ni and ^{48}Ca nuclei. It can be seen clearly that the theoretically estimates from HFB+HO model (with both UNEDF0 and UNEDF1 parameterizations) are nicely matching with the recently available experimental data. UNEDF0 parameterization are giving very good results of neutron skin thickness while UNEDF1 parameterization are producing even better results of skin thickness for the doubly magic nuclei with higher mass number as we can see in the Fig. For lower mass number range, the result of UNEDF0 parameterization is overestimated by approximately 0.03 fm (when compared with experimental data) and almost matching (when compared with experimental data) for ^{48}Ca . Also for ^{68}Ni , our result calculated with UNEDF0 parameterization is overestimated by approximately 0.09 fm and 0.1 fm (when both result are compared with the experimental data taken from). The results that we have computed here are taken from Axially deformed solution of the Skyrme-Hartree-Fock-Bogoliubov equations using the harmonic oscillator model (HFB+HO) based on Energy Density Functional (EDF) parameterizations UNEDF0 and UNEDF1.

4. Conclusions

By employing Nuclear Density Functionals based on HFB+HO model parameterizations (UNEDF0 and UNEDF1) on various nuclei, we have reached to some striking conclusions, which are discussed in this section.

The theoretically computed results with NDF parameterizations (UNEDF0 and UNEDF1) for nuclear root-mean-square radii R_{rms} , charge radii R_{ch} and neutron skin thickness Δr_{np} defined in Eq. (8) are presented and compared with recent available experimental data. It can be extracted from Fig. (9) that the ratio $Z/N \approx 0.7$ in doubly magic nuclei ^{48}Ca , ^{120}Sn and ^{208}Pb and the value of Δr_{np} lies in close order of 0.16-0.19 fm, whereas for the ratio $Z/N \approx 0.5-0.6$ in ^{42}Si , ^{44}S and ^{132}Sn , the value of Δr_{np} is more than 0.25 fm. This observation establishes the relationship of ratio Z/N with

Δr_{np} in the doubly magic and neutron rich nuclei indicating shell closures in the recent investigations [52] in ^{42}Si nucleus. The charge radii for Si, S, Ar and Ca isotopes is observed to be minimum at neutron number $N=14$. The small magnitudes of R_c in ^{28}Si , ^{30}S , ^{32}Ar and ^{34}Ca nuclei suggests $N=14$ as a new magic number. The theoretically computed results are reasonably reproducing the values for Δr_{np} in ^{208}Pb , $^{120,132}\text{Sn}$, and ^{68}Ni nuclei are in the ranges 0.13 - 0.19 fm, 0.12 - 0.16 fm, and 0.15 - 0.19 fm, respectively from ref. [59], whereas the in case of ^{48}Ca , our results overestimated by very small value of approximately 0.01 fm only. These results confirms the validity of skyrme-interactions with zero range pairing spin interactions for the exotic nuclei.

5. Acknowledgements

Author(s) would like to thank Himachal Pradesh University for providing computational facilities, DST- INSPIRE for providing financial assistance (Junior Research Fellowship) and anonymous referee(s) for extremely thorough inspection of the manuscript and helpful comments.

REFERENCES

- [1] E. Lunderberg, et al. In-beam γ -ray spectroscopy of $^{38-42}\text{S}$. *Phys. Rev. C*, 94:064327, Dec 2016.
- [2] A. Gade, et al. In-beam γ -ray spectroscopy of very neutron-rich nuclei: Excited states in ^{46}S and ^{48}Ar . *Phys. Rev. Lett.*, 102:182502, May 2009.
- [3] L. Coraggio, et al. Spectroscopic study of neutron-rich calcium isotopes with a realistic shell-model interaction. *Phys. Rev. C*, 80:044311, Oct 2009.
- [4] Panagiota Papakonstantinou, et al. Density dependence of the nuclear energy-density functional. *Phys. Rev. C*, 97:014312, Jan 2018.
- [5] T. Nikšić, et al. Relativistic nuclear energy density functionals: Adjusting parameters to binding energies. *Phys. Rev. C*, 78:034318, Sep 2008.
- [6] M. Bhuyan, et al. Surface properties of neutron-rich exotic nuclei within relativistic mean field formalisms. *Phys. Rev. C*, 97:024322, Feb 2018.
- [7] A. Gade, et al. Cross-shell excitation in two-proton knockout: Structure of ^{52}Ca . *Phys. Rev. C*, 74:021302, Aug 2006.
- [8] Yutaka Utsuno, et al. Shape transitions in exotic si and s isotopes and tensor-force-driven jahn-teller effect. *Phys. Rev. C*, 86:051301, Nov 2012.
- [9] J. A. Tostevin, et al. Two-proton removal from ^{44}s and the structure of ^{42}si . *Phys. Rev. C*, 87:027601, Feb 2013.
- [10] S. Bhattacharyya, et al. Structure of neutron-rich ar isotopes beyond $n=28$. *Phys. Rev. Lett.*, 101:032501, Jul 2008.

- [11] Yutaka Utsuno, et al. Nature of isomerism in exotic sulfur isotopes. *Phys. Rev. Lett.*, 114:032501, Jan 2015.
- [12] S. R. Stroberg, et al. Single-particle structure of silicon isotopes approaching ^{42}Si . *Phys. Rev. C*, 90:034301, Sep 2014.
- [13] O. Sorlin, et al. Decay properties of exotic $n \simeq 28$ s and cl nuclei and the $^{48}\text{Ca}/^{46}\text{Ca}$ abundance ratio. *Phys. Rev. C*, 47:2941–2953, Jun 1993.
- [14] R Schneider, et al. Production and identification of 100 sn. *Zeitschrift für Physik A Hadrons and Nuclei*, 348(4):241–242, 1994.
- [15] G Leander and SE Larsson. Potential-energy surfaces for the doubly even $n = z$ nuclei. *Nuclear Physics A*, 239(1):93–113, 1975.
- [16] HR Jaqaman and L Zamick. High multipole moments in nuclei. *Physical Review C*, 30(5):1719, 1984.
- [17] H Flocard, et al. Configuration space, cranked hartree-fock calculations for the nuclei 16o, 24mg and 32s. *Progress of Theoretical Physics*, 72(5):1000–1016, 1984.
- [18] M. Girod and B. Grammaticos. *Phys. Rev. C*, **27**:2317, 1983.
- [19] RJ Furnstahl. Rj furnstahl, ce price, and ge walker, phys. rev. c 36, 2590 (1987). *Phys. Rev. C*, 36:2590, 1987.
- [20] J Fink, et al. Systematic study of potential energy surfaces of light nuclei in relativistic hartree calculations. *Physics Letters B*, 218(3):277–282, 1989.
- [21] SK Patra and CR Praharaaj. Shapes of $n = z$ nuclei in the mass $a = 20$ –48 region. *Nuclear Physics A*, 565(2):442–454, 1993.
- [22] Jian-Kang Zhang and DS Onley. Systematic relativistic hartree-fock calculation of deformed nuclei in s-d shell. *Physical Review C*, 49(2):762, 1994.
- [23] M Carchidi, BH Wildenthal, and B Alex Brown. Quadrupole moments of sd-shell nuclei. *Physical Review C*, 34(6):2280, 1986.
- [24] J Zhang, WDM Rae, and AC Merchant. Systematics of some 3-dimensional α -cluster configurations in $4n$ nuclei from 16o to 44ti. *Nuclear Physics A*, 575(1):61–71, 1994.
- [25] Junjie Yang and J. Piekarewicz. Difference in proton radii of mirror nuclei as a possible surrogate for the neutron skin. *Phys. Rev. C*, 97:014314, Jan 2018.
- [26] B. Alex Brown. Mirror charge radii and the neutron equation of state. *Phys. Rev. Lett.*, 119:122502, Sep 2017.
- [27] B. A. Brown, et al. Calculations of the neutron skin and its effect in atomic parity violation. *Phys. Rev. C*, 79:035501, Mar 2009.
- [28] M Centelles, et al. Nuclear symmetry energy probed by neutron skin thickness of nuclei. *Physical review letters*, 102(12):122502, 2009.
- [29] M. Kortelainen, et al. *Phys. Rev. C*, **85**:024304, 2012.
- [30] M.V. Stoitsov, et al. *Computer Physics Communications*, **167**:43–63, 2005.
- [31] M. Kortelainen, T. Lesinski, J. Moré, W. Nazarewicz, J. Sarich, N. Schunck, M. V. Stoitsov, and S. Wild. Nuclear energy density optimization. *Phys. Rev. C*, 82:024313, Aug 2010

- [32] Peter Ring and Peter Schuck. *The nuclear many-body problem*. Springer Science & Business Media, 2004.
- [33] Michael Bender, Paul-Henri Heenen, and Paul-Gerhard Reinhard. Self-consistent mean-field models for nuclear structure. *Reviews of Modern Physics*, 75(1):121, 2003.
- [34] THR Skyrme. Thr skyrme, nucl. phys. 9, 615 (1959). *Nucl. Phys.*, 9:615, 1959.
- [35] H.J. Lipkin. *Ann. Phys.*, **9**:272, 1960.
- [36] J. Dobaczewski and W. Nazarewicz. *Phys. Rev. C*, **47**:2418, 1993.
- [37] M.V. Stoitsov, N. Schunck, M. Kortelainen, N. Michel, H. Nam, E Olsen, J. Sarich, and S. Wild. *Computer Physics Communications*, **184**:1592–1604, 2013.
- [38] R. F. Garcia Ruiz, et al, Unexpectedly large charge radii of neutron-rich calcium isotopes, *Nature Physics* 12 (2016) 594–598. doi:10.1038/nphys3645. URL <http://dx.doi.org/10.1038/nphys3645>
- [39] B. Bastin and S. Grévy. Collapse of the $n = 28$ shell closure in ^{42}Si . *Phys. Rev. Lett.*, **99**:022503, Jul 2007.
- [40] P. G. Reinhard, W. Nazarewicz, Information content of a new observable: The case of the nuclear neutron skin, *Physical Review C - Nuclear Physics* 81 (5). arXiv:1002.4140, doi:10.1103/PhysRevC.81.051303.
- [41] P.-G. Reinhard and W. Nazarewicz. Nuclear charge and neutron radii and nuclear matter: trend analysis. *arXiv:1601.06324v1 [nucl-th]*, Jan 2016.
- [42] G. Hagen, et al. Charge, neutron, and weak size of the atomic nucleus. *Nat Phys, Advance Online Publication/arXiv:1509.07169 [nucl-th]*, 2015.
- [43] I. Angeli and K.P. Marinova. Table of experimental nuclear ground state charge radii: An update. *Atomic Data and Nuclear Data Tables*, **99**(1):69–95, 2013.
- [44] B. K. Agrawal, Shashi K. Dhiman, and Raj Kumar. Exploring the extended density-dependent skyrme effective forces for normal and isospin-rich nuclei to neutron stars. *Phys. Rev. C*, **73**:034319, Mar 2006.
- [45] James M. Lattimer and Yeunhwan Lim. Constraining the symmetry parameters of the nuclear interaction. *The Astrophysical Journal*, **771**(1):51, 2013.
- [46] T. Niksic, N. Paar, D. Vretenar, and P. Ring. Dirhba relativistic self-consistent mean-field framework for atomic nuclei. *Computer Physics Communications*, **185**(6):1808–1821, 2014.
- [47] A. Tamii, et al. Complete electric dipole response and the neutron skin in ^{208}Pb . *Phys. Rev. Lett.*, **107**:062502, Aug 2011.
- [48] T. Hashimoto, et al. Dipole polarizability of ^{120}Sn and nuclear energy density functionals. *arXiv:1503.08321 [nucl-ex]*, 2015.
- [49] D. M. Rossi, et al. Measurement of the dipole polarizability of the unstable neutron-rich nucleus ^{68}Ni . *Phys. Rev. Lett.*, **111**:242503, Dec 2013.
- [50] W. Nazarewicz, et al. Symmetry energy in nuclear density functional theory. *The European Physical Journal A* **50**:20, Feb 2014.

- [51] T. Baumann, et al. Discovery of ^{40}Mg and ^{42}Al suggests neutron drip-line slant towards heavier isotopes. *Nature*, **449**:1022–1024, oct 2007.
- [52] J. Fridmann, et al. Magic nucleus ^{42}Si . *Nature*, **435**:922–924, June 2005.
- [53] J. Piekarewicz, B. K. Agrawal, G. Colò, W. Nazarewicz, N. Paar, P.-G. Reinhard, X. Roca-Maza, and D. Vretenar. Electric dipole polarizability and the neutron skin. *Phys. Rev. C*, **85**:041302, Apr 2012.
- [54] Lie-Wen Chen, Che Ming Ko, and Bao-An Li. Nuclear matter symmetry energy and the neutron skin thickness of heavy nuclei. *Phys. Rev. C*, **72**:064309, Dec 2005.
- [55] B. Kłos, et al. Neutron density distributions from antiprotonic ^{208}Pb and ^{209}Bi atoms. *Phys. Rev. C*, **76**:014311, Jul 2007.
- [56] E. Friedman. Neutron skins of ^{208}Pb and ^{48}Ca from pionic probes. *Nuclear Physics A*, **896**:46 – 52, 2012.
- [57] C. M. Tarbert, et al. Neutron skin of ^{208}Pb from coherent pion photoproduction. *Phys. Rev. Lett.*, **112**:242502, Jun 2014.
- [58] J. Zenihiro, et al. Neutron density distributions of $^{204,206,208}\text{Pb}$ deduced via proton elastic scattering at $E_p = 295$ mev. *Phys. Rev. C*, **82**:044611, Oct 2010.
- [59] X. Roca-Maza, et al. Neutron skin thickness from the measured electric dipole polarizability in ^{68}Ni , ^{120}Sn , and ^{208}Pb . *Phys. Rev. C*, **92**:064304, Dec 2015.
- [60] B. Alex Brown, et al. Neutron skin deduced from antiprotonic atom data. *Phys. Rev. C*, **76**:034305, Sep 2007.
- [61] M. Wang, et al. The ame2012 atomic mass evaluation. *Chinese Physics C*, **36**:1603–2014, 2012.
- [62] A. Klimkiewicz, et al, Nuclear symmetry energy and neutron skins derived from pygmy dipole resonance. *Phys. Rev. C* 76 (2007) 051603. doi:10.1103/PhysRevC.76.051603. URL <https://link.aps.org/doi/10.1103/PhysRevC.76.051603>
- [63] J. M. Dong, L. J. Wang, W. Zuo, J. Z. Gu, Constraints on Coulomb energy, neutron skin thickness in ^{208}Pb , and symmetry energy, *Physical Review C* 97 (3) (2018) 034318. doi:10.1103/PhysRevC.97.034318. URL <https://link.aps.org/doi/10.1103/PhysRevC.97.034318>
- [64] X. Roca-Maza, et al, Electric dipole polarizability in ^{208}Pb : Insights from the droplet model, *Physical Review C - Nuclear Physics* 88 (2) (2013) 1–7. arXiv:1307.4806, doi:10.1103/PhysRevC.88.024316.
- [65] M. H. Mahzoon, M. C. Atkinson, R. J. Charity, W. H. Dickhoff, Neutron skin thickness of ^{48}Ca from a nonlocal dispersive optical-model analysis, *Phys. Rev. Lett.* 119 (2017) 222503. doi:10.1103/PhysRevLett.119.222503. URL <https://link.aps.org/doi/10.1103/PhysRevLett.119.222503>

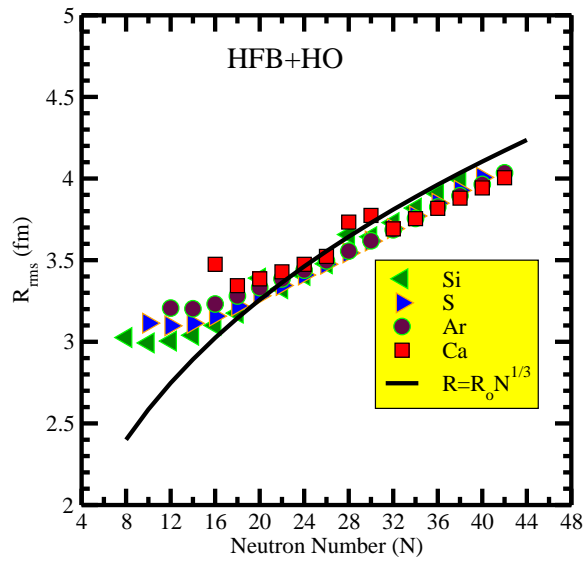


Fig. 1. (color online) The root mean square radius in fm plotted as a function of Neutron Number (N), for the exotic nuclei of Silicon, Sulphur, Argon and Calcium. The theoretical estimates are computed from Axially deformed solution of the Skyrme-Hartree-Fock-Bogoliubov equations using the harmonic oscillator basis (HFB+HO), based on Energy Density Functional (EDF) parameterization UNEDF0.

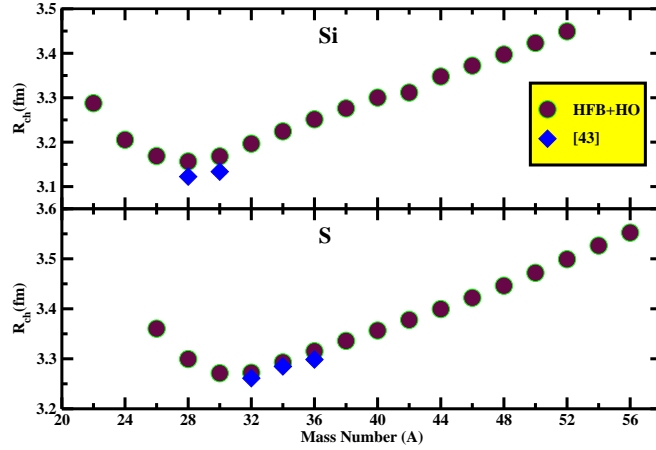


Fig. 2. (color online) The charge radius in fm plotted as a function of Mass Number (A), for the exotic nuclei of Silicon (upper panel) and Sulphur (lower panel). The theoretical estimates are computed from Axially deformed solution of the Skyrme-Hartree-Fock-Bogoliubov equations using the harmonic oscillator basis (HFB+HO), based on Energy Density Functional (EDF) parameterization UNEDF0. The experimental data is taken from [43].

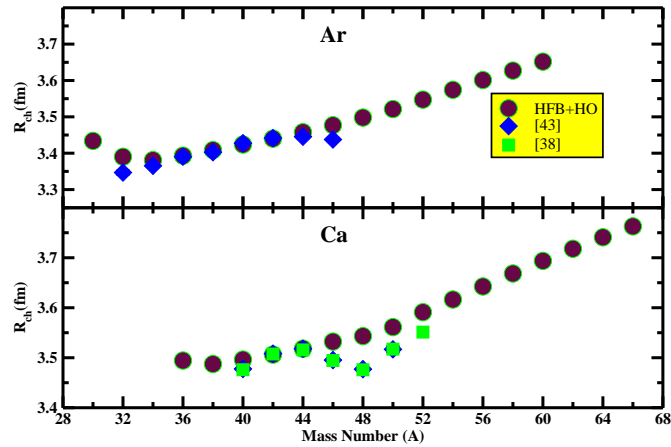


Fig. 3. (color online) The charge radius in fm plotted as a function of Mass Number (A), for the exotic nuclei of Argon (upper panel) and Calcium (lower panel). The theoretical estimates are computed from Axially deformed solution of the Skyrme-Hartree-Fock-Bogoliubov equations using the harmonic oscillator basis (HFB+HO), based on Energy Density Functional (EDF) parameterization UNEDF0. The experimental data is taken from [43, 38].

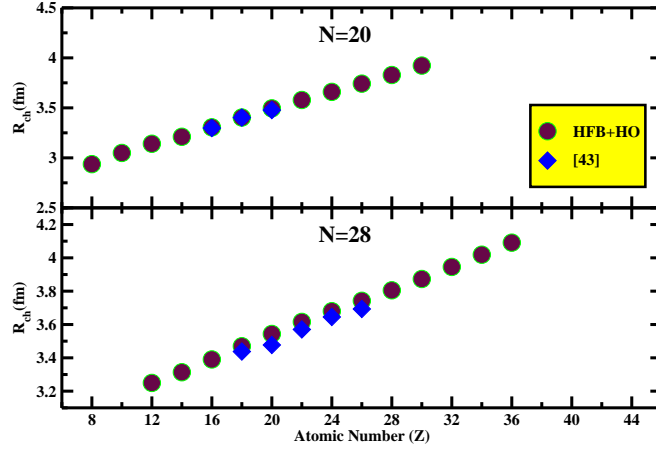


Fig. 4. (color online) The charge radius in fm plotted as a function of Atomic Number (Z), for the exotic nuclei of $N = 20$ (upper panel) and $N = 28$ (lower panel) isotones. The theoretical estimates are computed from Axially deformed solution of the Skyrme-Hartree-Fock-Bogoliubov equations using the harmonic oscillator basis (HFB+HO), based on Energy Density Functional (EDF) parameterization UNEDF0. The experimental data is taken from [43].

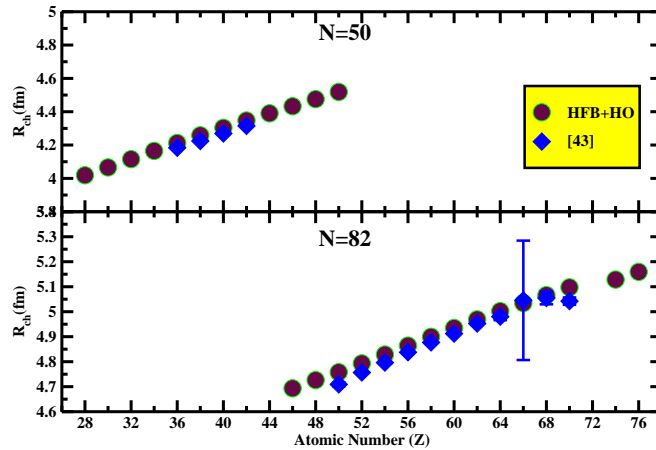


Fig. 5. (color online) The charge radius in fm plotted as a function of Atomic Number (Z), for the exotic nuclei of $N = 50$ (upper panel) and $N = 82$ (lower panel) isotones. The theoretical estimates are computed from Axially deformed solution of the Skyrme-Hartree-Fock-Bogoliubov equations using the harmonic oscillator basis (HFB+HO), based on Energy Density Functional (EDF) parameterization UNEDF0. The experimental data is taken from [43].

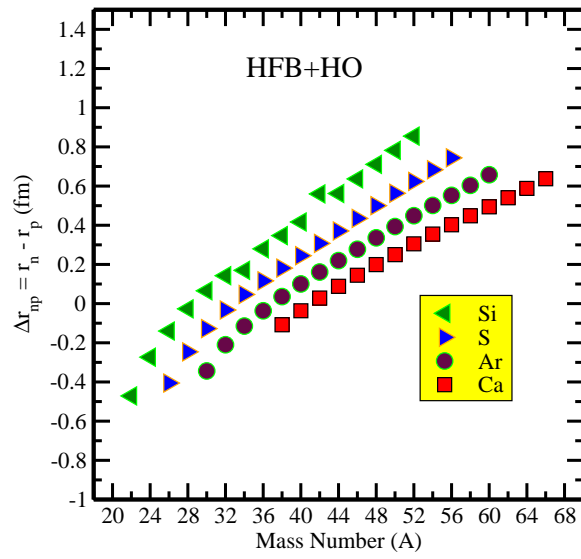


Fig. 6. (color online) The neutron skin thickness $\Delta r_{np} = r_n - r_p$ in fm, plotted as a function of Mass Number (A), for the chain of isotopes of Silicon, Sulphur, Argon and Calcium. The theoretical estimates are computed from Axially deformed solution of the Skyrme-Hartree-Fock-Bogoliubov equations using the harmonic oscillator basis (HFB+HO), based on Energy Density Functional (EDF) parameterization UNEDF0.

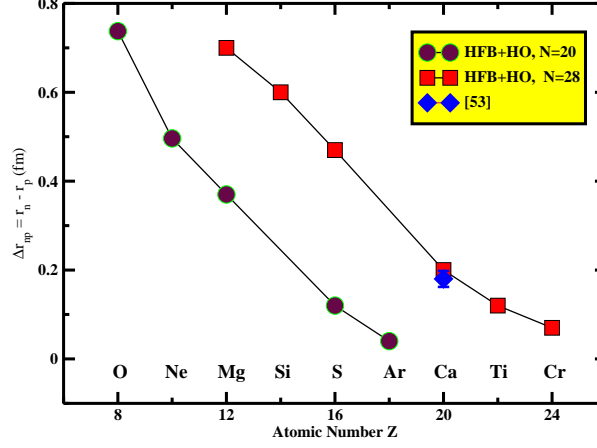


Fig. 7. (color online) The neutron skin thickness $\Delta r_{np} = r_n - r_p$ in fm, plotted as a function of Atomic Number (Z), for the isotonic chain of of $N = 20$ and $N = 28$. The theoretical estimates are computed from Axially deformed solution of the Skyrme-Hartree-Fock-Bogoliubov equations using the harmonic oscillator basis (HFB+HO), based on Energy Density Functional (EDF) parameterization UNEDF0.

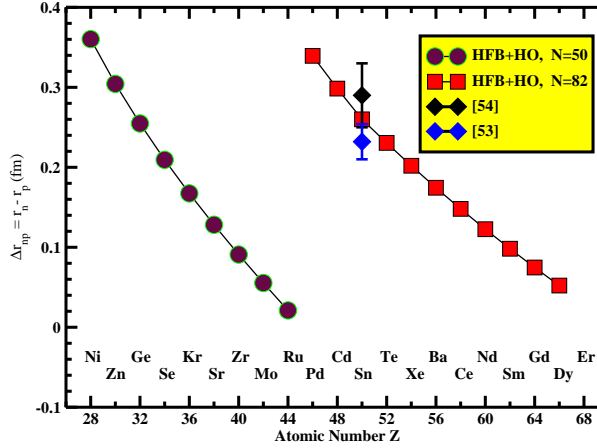


Fig. 8. (color online) The neutron skin thickness $\Delta r_{np} = r_n - r_p$ in fm, plotted as a function of Atomic Number (Z), for the isotonic chain of of $N = 50$ and $N = 82$. The theoretical estimates are computed from Axially deformed solution of the Skyrme-Hartree-Fock-Bogoliubov equations using the harmonic oscillator basis (HFB+HO), based on Energy Density Functional (EDF) parameterization UNEDF0.

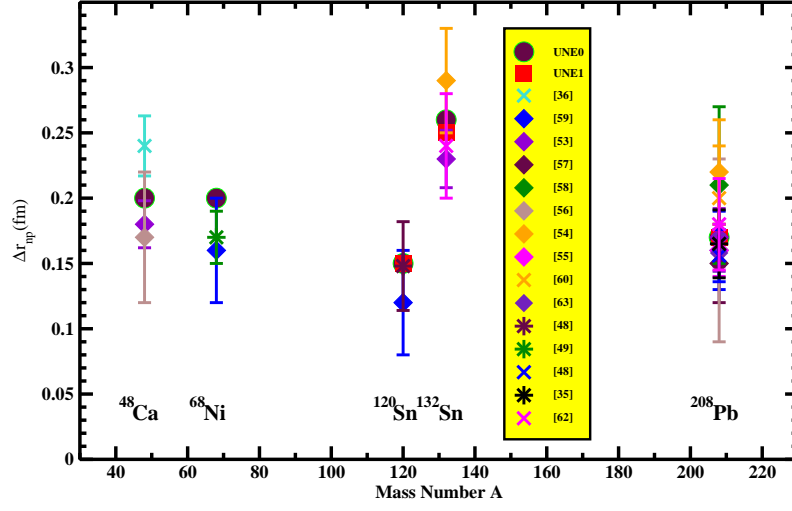


Fig. 9. (color online) Neutron skin thickness $\Delta r_{np} = r_n - r_p$ in fm calculated theoretically for doubly magic nuclei. The theoretical estimates are computed from Axially deformed solution of the Skyrme-Hartree-Fock-Bogoliubov equations using the harmonic oscillator basis (HFB+HO), based on Energy Density Functional (EDF) parameterization UNEDF0 and UNEDF1. Data is also listed from the different experimental and theoretical results.